FLOW NON-UNIFORMITY AND HEAT TRANSFER IN ANNULAR PLATE-FIN RADIATOR

Zhiying Liu[1], Hui Li[1]*,Yuanyuan Zhou[1], Haifeng Jiang[1], Lin Shi[1], Yangjun Zhang[2], Jiawei Wang[2]
(1. Key Laboratory for Thermal Sciences and Power Engineering of the Ministry of Education, Tsinghua University, Beijing 100084, China
2. State Key Laboratory of Automotive Safety and Energy, Tsinghua University, Beijing 100084, China)
*Author for correspondence
Key Laboratory for Thermal Sciences and Power Engineering of the
Ministry of Education, Tsinghua University,
Beijing, 100084,
China,
E-mail: hui-li@mail.tsinghua.edu.cn

ABSTRACT

Annular radiators can be used for heavy-duty vehicle engine cooling systems, domestic air conditioning, and electronic devices cooling system. A test apparatus was set up to investigate the flow and heat transfer characteristics in annular radiators. An infrared camera was used to measure the temperature distribution. The experimental results show that the temperature is not uniform along the radiator height because of the air flow non-uniformity. The internal flow field was numerically investigated and a variable fin pitch optimization method was presented to reduce the flow non-uniformity. The porous medium model was used to predict the radiator pressure drop. The simulation accuracy was verified by the experimental data. The numerical results show that the flow non-uniformity is greatly influenced by the fan diameter and height ratio and can be reduced by the variable fin pitch method.
Key-words: annular radiator, flow non-uniformity, heat transfer, porous medium model.

INTRODUCTION

With the engines and electronic devices having higher power densities and being more compact, the cooling systems for heavy vehicles are also becoming more compact and efficient. However, the reduction of the size can affect the flow and heat transfer. In a conventional duct (Figure 1), the severe constriction of the intake duct leading to an uneven flow field and a large region with slow air flow. Oliet et al. [1] analysed the influence of the parameters on the thermal and hydraulic behaviour of the heat exchanger and provided a detailed example of the overall behaviour of an automobile radiator working at usual range of operating conditions. Witry et al. [2] studied a patterned plate heat exchanger using the CFD code FLUENT to predict the internal flow. Chong et al. [3] analysed the heat rejection rate in the function of temperature difference between the radiators and the ambient for different water flow rates and wind speeds created by the fan using CFD program and analytical formulas. Other studies have analysed the air-side thermal hydraulic performance of various kinds of heat exchangers [4-7]. Saidi et al. [8] studied the radiator performance for passenger car. However, there is few domestic research on annular radiators, and relevant experimental data is inadequate. The inlet airflow direction was not yet considered.

A cooling system with annular radiator and multi-blade centrifugal fan shown in Figure 2 is tested in this paper to study on the non-uniformity of flow and heat transfer. Based on the experimental data, the internal flow field was numerically investigated for radiators with different diameter and height ratio. The porous media model is used to predict the radiator pressure drop. A variable fin pitch optimization method was presented to reduce the flow non-uniformity.

NOMENCLATURE

A	[m^2]	Heat transfer area of the radiator
c_p	[J/kgK]	Specific heat
d_h	[m]	Hydraulic diameter of the air-side
Fp	[mm]	Fin pitch
Fh	[mm]	Fin height
g_c	[m/s2]	Acceleration of gravity
h	[W/m^{2}K]	Convective heat transfer coefficient
K	[W/m^{2}K]	Interfacial heat transfer coefficient
L	[m]	Length along the air flow
$\dot{m}$	[kg/s]	Mass flow rate
ΔP	[Pa]	Pressure drop
Q	[kW]	Heat transfer rate
T	[K]	Temperature
U,u	[m/s]	Velocity
Greek symbols		
η	[%]	Fin efficiency
λ	[W/mK]	Thermal conductivity

τ	[Pa]	Wall shear stress

Subscripts

c		Cold fluid side(air-side)
h		Hot fluid side(water-side)
m		Arithmetic mean value
min		Maximum
max		Minimum
x		X-axis component
y		Y-axis component
z		Z-axis component

EXPERIMENT DETAILS

Test apparatus is set up to investigate flow and heat transfer characteristics of the annular radiators. Heat transfer rate and pressure drop are measured to test the radiator performance. Temperature distribution along the radiator height is obtained by an infrared camera.

Test Apparatus

Figure 3 shows a schematic of the test apparatus used in this study. The system consisted of an inlet duct, an annular radiator , heat transfer fluid (water) circulation and control units, and a data collection system and measurement instruments. The inlet of the air-side of the annular radiator is maintained by controlling the centrifugal fan.The air flow rate was measured by a hot-wire anemometer in the inlet duct. The air-side pressure drop across the annular radiator was measured by a U-type pressure gauge. The heat transfer fluid circulation and control units maintained the inlet at the water-side by regulating the water flow rate and inlet temperature. An infrared camera was used to measure the temperature distribution on the outside of the annular radiator. The uncertainties of the measurement instruments are listed in Table 1.
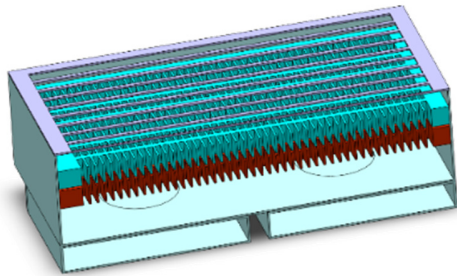

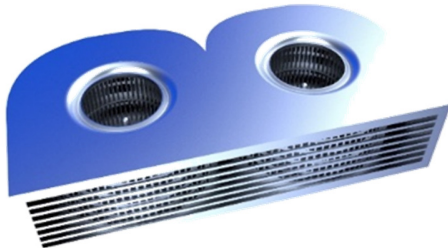**Figure 1** Conventional cooling system.

Figure 2 Cooling system with annular radiator.

The annular radiator had serrated fins in the air-side and flat tubes in the water-side. The outside diameter diameter was 310mm and the inside diameter was 222 mm. The height is 130 mm. The fin pitch was 3 mm, the fin length was 10 mm, and the fin height was 10 mm.

Test condition and method

The tests were performed at low Reynolds numbers, based on the hydraulic diameter and mean velocity of 4-8 m/s, and a water flow rate of 5 L/min. The air inlet temperature was 27 ℃ and the water inlet temperatures was 50℃.

Data Processing

The heat transfer rate was expressed as

$$Q = c_{p,h} \dot{m}_h \Delta T_h \qquad (1)$$

Where $c_{p,h}$ is the constant pressure specific heat on the water side, $\dot{m}_h$ is the water mass flow rate, and ΔT_h is the difference between the inlet and outlet water temperatures.

The air flow rate was calculated by

$$\dot{m}_c = \frac{1}{4}\pi d_c^2 U_c \qquad (2)$$

Where d_c is the inlet duct diameter, and U_c is the velocity measured by the hot-wire anemometer.
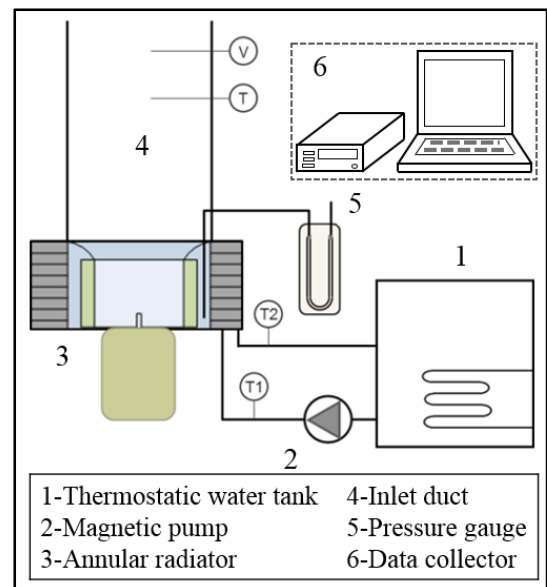
The temperature difference in the air side was

$$\Delta T_c = \frac{Q}{c_{p,c}\dot{m}_c} \qquad (3)$$

Where $c_{p,c}$ is the constant pressure specific heat on the air side and $\dot{m}_c$ is the air mass flow rate.

Table 1   The uncertainty of measuring instruments.

Measuring instruments	uncertainty
Thermal resistor [℃]	0.1
hot-wire anemometer [m/s]	0.05
U-type pressure gauge [Pa]	5
Infrared camera [℃]	2

1-Thermostatic water tank   4-Inlet duct
2-Magnetic pump   5-Pressure gauge
3-Annular radiator   6-Data collector

The logarithm mean temperature difference was expressed as

$$\Delta T_{\text{LMTD}} = \frac{\Delta T_{\text{max}} - \Delta T_{\text{min}}}{\ln(\Delta T_{\text{max}}/\Delta T_{\text{mix}})} \quad (4)$$

The total heat transfer coefficient based on the air-side heat transfer area was expressed as

$$K = \frac{Q}{A_c \Delta T_{\text{LMTD}}} \quad (5)$$

Where A_c is the air-side heat transfer area.

The air-side heat transfer coefficient was separated from the total heat transfer coefficient as

$$h_c = \frac{1}{\eta_{oc}(\frac{1}{K} - \frac{A_c}{A_h}\frac{1}{h_h} - \frac{A_c}{A_h}\frac{\delta}{\lambda})} \quad (6)$$

Where η_{oc} is the air-side fin efficiency, h_h is the water-side convective heat transfer coefficient, A_h is the water-side heat transfer area, δ is the fin thickness, and λ is the fin thermal conductivity.

The j factor, f factor and Nusselt number was calculated as

$$j = StPr^{2/3} = \frac{Nu}{RePr^{1/3}} \quad (7)$$

$$f = \frac{\tau_w}{\rho u_m^2/2g_c} \quad (8)$$

Where τ_w is the wall friction stress, ρ is the air density, u_m is the mean velocity of the air flow, and g_c is the acceleration of gravity.

The heat transfer and pressure drop was nondimensionalized to the f and j factor correlations as

$$j = 0.2217Re^{-0.409} \quad (9)$$

$$f = 6.0145Re^{-0.653} \quad (10)$$

Figure 4 campared the experimental data with the relevant literature [9]. The deviations of j, f factor are within 30%.
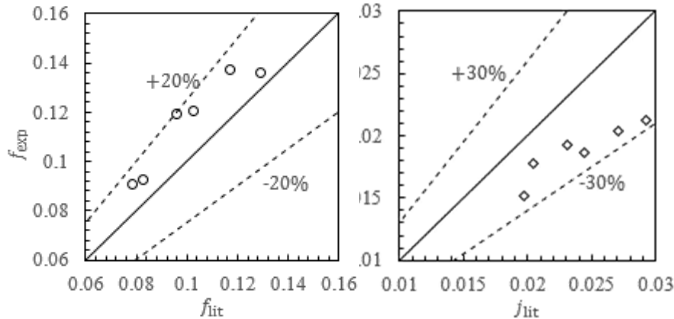
**Figure 4** Comparison of experimental data with relevant literature [9] for j, f factor.

Temperature distribution

Figure 5 shows the temperature distribution on the outside of the annular radiator. Temperature is unevenly distributed along the height direction. It is almost like the water temperature at the top, while some temperature at the bottom is much lower. As the annular radiator is assembled very close to the centrifugal fan, it can be inferred that air flow rate is uneven along the height direction because the diameter and height ratio of the centrifugal fan is too small.

SIMULATION DETAILS

Since the temperature distribution is related to the local air flow rate and the internal flow field cannot be experimentally observed, the 3-D simulations were used to investigate the air flow non-uniformity. The simplified cooling system contains an annular radiator and a multi-blade centrifugal fan. Two cases of different diameter and height ratios were computed to analyse the flow field non-uniformity along the height direction.
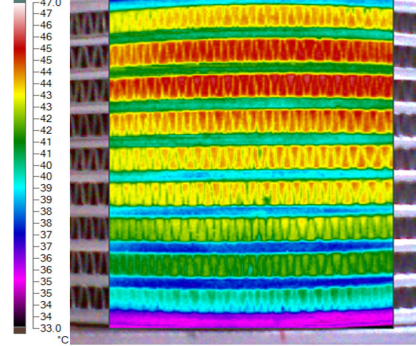

Figure 5 Temperature distribution on the outside of the annular radiator.

Furthermore, the radiator fin pitch can be variable along the height direction to change the local pressure drop and adapt to the air flow non-uniformity. The fin pitch can increase at the top and decrease at the bottom to mitigate the flow non-uniformity. Another two cases were computed to study the variable fin pitch optimization method. As the radiator is very complex and the mesh number is amazing large, porous medium model is used to simplify the computing mesh. The parameters of porous medium model are determined by the experimental results and the linear and quadratic resistance coefficients model.

Geometry and mesh details

The computational domain of 3-D simulation is shown in Figure 6. A hemispheric inlet boundary and the annular outlet boundary is used to make the simulation approaching real situation. The multi-blade centrifugal fan diameters are 160 mm for all the cases, and the heights are 130 mm and 65 mm for different cases. There are 60 forward blades in the centrifugal fans. The radiator diameters are same as the experiment and the heights are same as the centrifugal fans. The fin parameters are the same as the experiment for case A and B. The fin pitches are variable for case C and D by dividing the radiator into three sub region along the height direction as shown in Figure 7. The parameters are listed in Table 2. The case A is same as the experiment radiator. The heat transfer rate calculated by the heat transfer correlations is the same for the cases to ensure the comparability.

The multi-blade centrifugal fan

Hemispheric inlet boundary

Outlet boundary

Annular radiator (porous medium model)
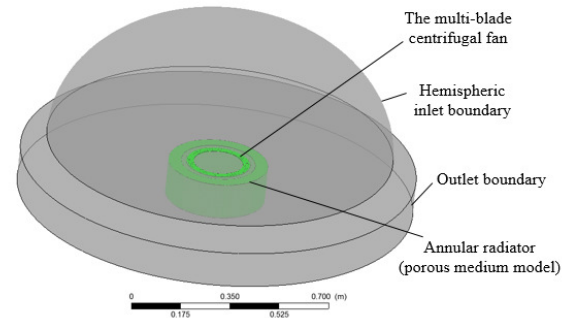
Figure 6 Computational domain of 3-D simulation.

Table 2 The radiator parameters.

Case No.	Height [mm]	Fin pitch in each sub region [mm]		
		Top	Middle	Bottom
Case A	130	3	3	3
Case B	65	3	3	3
Case C	130	4	3	2
Case D	65	4	3	2

(a) Constant fin pith   (b) Variable fin pitch
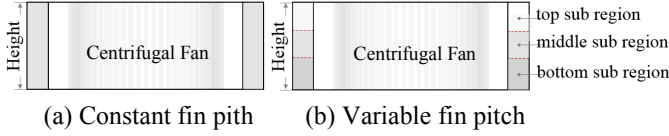
Figure 7 Geometry of the simulation cases.

Numerical method and computational details

The flow field and the pressure distribution in the cooling system were obtained by solving the continuity and momentum equations as

Continuity:

$$\frac{\partial \rho}{\partial t} + \nabla \cdot (\rho U) = 0 \tag{11}$$

Momentum:

$$\frac{\partial (\rho U)}{\partial t} + \nabla \cdot (\rho U \times U) = -\nabla p + \nabla \cdot \tau + S_M \tag{12}$$

Where the stress tensor τ is related to the strain rate by

$$\tau = \mu \left(\nabla U + (\nabla U)^T - \frac{2}{3} \delta \nabla \cdot U \right) \tag{13}$$

Since the heat transfer is not involved in the simulation, the energy equation was not solved in the simulation.

The radiator pressure drop was predicted using the directional porous medium model. The momentum loss through an anisotropic porous region can be modelled using the directional loss model. The momentum losses in the streamwise and transverse directions were

$$S_{M,x'} = -\frac{\mu}{K_{perm}^S} U_{x'} - K_{loss}^S \frac{\rho}{2} |U| U_{x'} \tag{14}$$

$$S_{M,y'} = -\frac{\mu}{K_{perm}^T} U_{y'} - K_{loss}^T \frac{\rho}{2} |U| U_{y'} \tag{15}$$

$$S_{M,z'} = -\frac{\mu}{K_{perm}^T} U_{z'} - K_{loss}^T \frac{\rho}{2} |U| U_{z'} \tag{16}$$

Where K_{perm}^S and K_{perm}^T are the streamwise and transverse permeabilities, K_{loss}^S and K_{loss}^T are the streamwise and transverse quadratic loss coefficients. The momentum loss source was formulated using linear and quadratic resistance coefficients as

$$K_L^S = \frac{\mu}{K_{perm}^S} \tag{17}$$

$$K_Q^S = K_{loss}^S \frac{\rho}{2} \tag{18}$$

$$K_L^T = \frac{\mu}{K_{perm}^T} \tag{19}$$

$$K_Q^T = K_{loss}^T \frac{\rho}{2} \tag{20}$$

Where K_L^S and K_L^T are the streamwise and transverse linear resistance coefficients, and K_Q^S and K_Q^T are the streamwise and transverse quadratic resistance coefficients. The pressure drop is modelled using:

$$\frac{\partial p}{\partial x_i} = -K_L U_i - K_Q |U| U_i \tag{21}$$

Where K_L and K_Q are the linear and quadratic resistance coefficients, U_i is the local velocity in the i direction, and $\frac{\partial p}{\partial x_i}$ is the pressure drop gradient in the i direction.

The inlet boundary was pressure inlet boundary, and the total pressure was set to 1 atm. The outlet boundary was pressure outlet boundary, and the average static pressure of the outlet was 1 atm. The fan was simulated using frozen rotor method and the rotating speeds were 500 to 1200 rpm at interval of 100 rpm. The volume porosity was set to the free flow area and frontal area ratio of the radiator. The streamwise direction in the porous region was the radial direction. The streamwise momentum loss were determined by the linear and quadratic resistance coefficients which were calculated by the secondary polynomial regressions of the experimental results. The transverse loss was 10 times than the streamwise.

RESULTS AND DISCUSSION

Since the experimental results were agreed with Wang's[9], the numerical results were compared with the experimental data to verify the accuracy as shown in Figure 8. The maximum difference is within 20%, and the trends are fit well. Figure 9 shows the air flow vector in the longitudinal section. The air is sucked into the centrifugal fan from the top then blowed to the annular radiator. There are vortexes in the upper part, which cause the air flow rate is not uniform along the height direction. The flow non-uniformity can influence both the heat transfer and pressure drop.
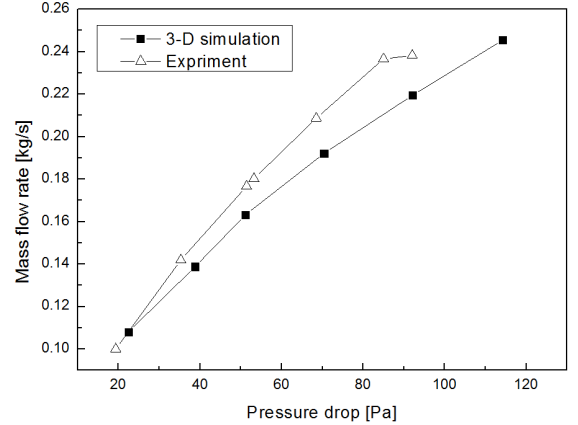
Figure 8 Comparison of 3-D simulation results with experimental data.
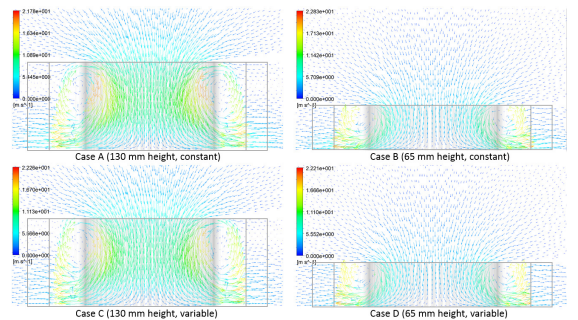
Figure 9 Velocity vector in the longitudinal section.

Air flow distribution

Figure 10 shows the air flow distribution along the height direction for the simulation cases. The mass flow rate percentages are defined as:

$$G^* = \frac{G_z}{G_{tot}} \times 100\% \qquad (22)$$

Where G_{tot} is the total mass flow rate, G_z is the local mass flow rate, z is the nondimensional height defined as:

$$h^* = \frac{h}{H} \qquad (23)$$

Where H is the radiator height and h is the distance above the radiator bottom.

The flow distribution is the most non-uniform in case A and the most uniform in case D. The air flow rate is too low to take heat away in the upper part of the radiator. However, the air is flowing too fast at the bottom which causing large pressure drop. The flow distribution is much more uniform in case B and D. The results show that the fan height makes much stronger influence on the flow distribution than the variable fin pitch method. The variable fin pitch method can mitigate the flow non-uniformity.
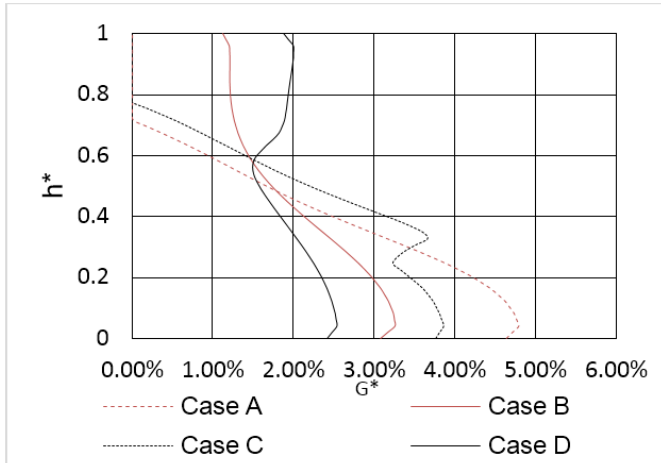

Figure 10   Comparison of the air flow distribution along the height directions.

Heat transfer

The heat transfer rate was approximately calculated by the numerical data. Since the flow distribution was in uniform, and the fin pitch was variable, the radiator was divided into three sub regions. The air mass flow rate in each sub region was calculated using the mass flow rate percentages. The air velocity in each sub region was assumed to be a constant to calculate the j factor using equation (9). The heat transfer rate was calculated as

$$Nu = jRePr^{1/3} \qquad (24)$$

$$K \approx h_c = \frac{Nu\lambda}{d_e} \qquad (25)$$

$$Q = KA_c \Delta T_{\text{LMTD}} \qquad (26)$$

Figure 11 compared the heat transfer rate for the cases. The flow non-uniformity makes the valid heat transfer area much smaller and decreases the total heat transfer rate. There is little heat transfer in the top sub regions of case A and C. The heat transfer rate of case B and case D is a little less than case A while the height is just half of case A. The heat transfer rate in the top

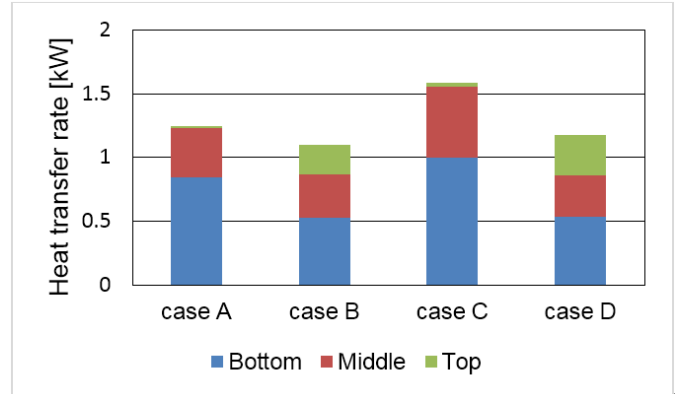sub region is greatly increased when using the variable fin pitch method.

Figure 11   Comparison of the heat transfer rate in sub regions.

Pressure drop

Figure 12 compared the cooling system pressure drop. The pressure drop is largely made by the air flow between the fan and radiator and the radiator fin channel. The variable fin pitch method can mitigate the flow non-uniformity and decrease the radiator pressure drop. However, the air flow between the fan and radiator becomes more complex increasing the pressure drop. The total pressure drop is almost the same for the four cases.
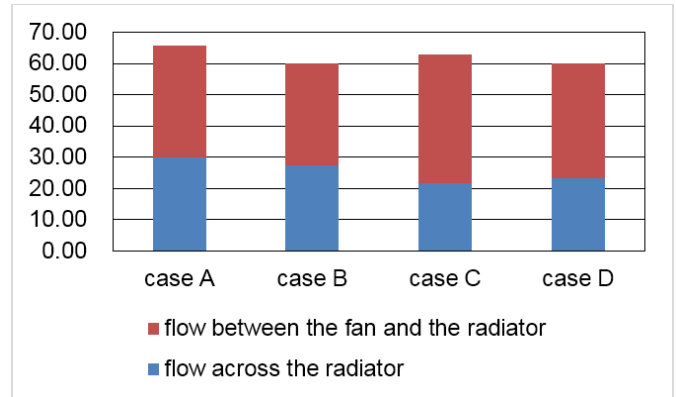

Figure 12   Comparison of the pressure drop.

CONCLUSION

Experiments on the annular radiator show that the flow field distribution and heat transfer are non-uniform along the height direction. The numerical results show that the flow non-uniformity along the height direction is greatly influenced by the diameter and height ratio. The large flow non-uniformity can make the valid heat transfer area much smaller and greatly lower the heat transfer rate. The variable fin pitch method can reduce the flow non-uniformity well and increase the heat transfer rate. The pressure drop is decreased when the diameter and height ratio is larger. The total pressure drop of the cooling system changes little when heat transfer is increased using the variable fin pitch method.

REFERENCESE

[1] Oliet C, Oliva A, Castro J, et al. Parametric studies on automotive radiators[J]. *Applied thermal engineering*, 2007, 27(11): 2033-2043.

[2] Witry A, Al-Hajeri M H, Bondok A A. Thermal performance of automotive aluminium plate radiator[J]. *Applied thermal engineering*, 2005, 25(8): 1207-1218.

[3] Chong K K, Tan W C. Study of automotive radiator cooling system for dense-array concentration photovoltaic system[J]. Solar Energy, 2012, 86(9): 2632-2643.

[4] Bell I H, Groll E A. Air-side particulate fouling of microchannel heat exchangers: experimental comparison of air-side pressure drop and heat transfer with plate-fin heat exchanger[J]. *Applied Thermal Engineering*, 2011, 31(5): 742-749.

[5] Kim M H, Bullard C W. Air-side thermal hydraulic performance of multi-louvered fin aluminum heat exchangers[J]. *International Journal of Refrigeration*, 2002, 25(3): 390-400.

[6] Kim M H, Bullard C W. Air-side performance of brazed aluminum heat exchangers under dehumidifying conditions[J]. *International Journal of refrigeration*, 2002, 25(7): 924-934.

[7] Chen H T, Lai S T, Haung L Y. Investigation of heat transfer characteristics in plate-fin heat sink[J]. *Applied Thermal Engineering*, 2013, 50(1): 352-360.

[8] Saidi M H, Mozafari A A, Sany A R E, et al. Experimental Study of Thermal Performance and Pressure Drop in Compact Heat Exchanger Installed in Automotive[C]. *ASME 2006 Internal Combustion Engine Division Spring Technical Conference. American Society of Mechanical Engineers*, 2006: 551-557.

[9] Wang Y Q, Dong Q W, Liu M S, et al. Numerical Study on Plate‐Fin Heat Exchangers with Plain Fins and Serrated Fins at Low Reynolds Number[J]. *Chemical engineering & technology*, 2009, 32(8): 1219-1226.

[10] Yang K S, Chiang C M, Lin Y T, et al. On the heat transfer characteristics of heat sinks: Influence of fin spacing at low Reynolds number region[J]. *International journal of heat and mass transfer*, 2007, 50(13): 2667-2674.

[11] Kays WM, London AL. Compact heat exchangers. 3rd ed. McGraw-Hill Book Company, 1984

[12] Aslam Bhutta M M, Hayat N, Bashir M H, et al. CFD applications in various heat exchangers design: A review[J]. *Applied Thermal Engineering*, 2012, 32: 1-12.